Powerful avidity with a limited valency for virus-attachment blockers on DC-SIGN: Combining chelation and statistical rebinding with structural plasticity of the receptor

Vanessa Porkolab,[†,a] Martin Lepšík[¶,x,a], Stefania Ordanini, [§,#] Alexander St John,[∂] Aline Le Roy, [†] Michel Thépaut,[†] Emanuele Paci,[¥] Christine Ebel, [†] Anna Bernardi,[§,#,*] Franck Fieschi[†,*]

[†] Univ. Grenoble Alpes, CNRS, CEA, Institut de Biologie Structurale, 38000 Grenoble, France. Email: franck.fieschi@ibs.fr

[¶] Univ. Grenoble Alpes, CNRS, CERMAV, 38000 Grenoble, France

[x] Institute of Organic Chemistry and Biochemistry, Czech Academy of Sciences, Flemingovo nam. 2, Prague 6, 166 10, Czechia

[§] Universita` degli Studi di Milano, Dipartimento di Chimica, via Golgi 19, 20133, Milano, Italy.

[#] CNR-ISTM, Inst. of Molecular Science and Technologies, Milano, Italy. Email: anna.bernardi@unimi.it

[∂] Astbury Centre & School of Molecular and Cellular Biology, University of Leeds, Leeds, UK

[¥] Department of Physics and Astronomy "Augusto Righi"

Keyword: C-type lectin receptors, multivalency, avidity, surface plasmon resonance, glycomimetics, chelation binding mode, molecular modelling, Emerging virus, SARS-CoV-2, Dengue.

[a] Both authors contributed equally

[*]Corresponding authors

Abstract : The C-type lectin receptors DC-SIGN and L-SIGN have been highlighted as co receptors for the spike protein of the SARS-CoV-2 virus. A multivalent glycomimetic ligand, Polyman26, has been described as able to inhibit DC-SIGN-dependent trans-infection of SARS-CoV-2. The molecular details underlying avidity generation in such system remain poorly characterized. In an effort to dissect the contribution of the known multivalent effects of Polyman26 - chelating, clustering and statistical rebinding – we studied a series of dendrimer constructs with a rod core rationally designed to engage simultaneously two binding sites of the tetrameric dendritic cell lectin receptor DC-SIGN. Different binding properties of these compounds have been studied with a range of biophysical techniques. Using molecular modelling we addressed, for the first time, the impact of the carbohydrate recognition domains' flexibility of the DC-SIGN tetramer on the compounds' avidity. We were able to gain deeper insight into the role of different binding modes, which in combination produce a construct with a nM affinity despite a limited valency. This multi-faceted experimental-theoretical approach provide detailed understanding of multivalent ligand/multimericprotein interactions which can lead to future predictions. This work opens the way to the development of new virus attachment blockers adapted to different C-type lectin receptors of viruses.

Introduction

Multivalency is commonly used by Nature to boost the intrinsically weak affinities of carbohydrates towards their lectin receptors. This also happens with C-type lectin receptors (CLRs) which bind glycans in a Ca^{2+}-dependent fashion. The spatial proximity of carbohydrate recognition domains (CRDs) in oligomeric CLRs can be leveraged for multivalent binding. Amongst CLRs, the dendritic cell membrane receptor DC-SIGN plays numerous roles in human immune system[1] interacting with specific carbohydrate structures (fucose, Lewis-type and high-mannose moieties) expressed on self-glycoproteins[2] and pathogens.[3–6][7]

DC-SIGN oligomerizes as homo-tetramer thanks to an extracellular coiled-coil region (Figure 1A and B) and include at the C-terminus of each monomer, a CRD containing the Ca^{2+}-dependent carbohydrate binding site.[8,9] Natural ligand affinity for individual CRD is weak (mM range). In the quest to compete against pathogens binding, or to modulate the immune responses due to DC-SIGN, numerous carbohydrate-based ligands were designed which bound to its CRD.[10–13] These efforts have led to the development of optimized glycomimetics with affinity down to the µM range.[14,15][16] However, the oligomerization of four CRDs, within the extracellular domain (ECD), enables to enhance the interaction strength with multivalent ligand through avidity phenomenon.[17,18] Thus, adding further multivalent display of these "glycomimetic spearheads" lead to improving binding avidities in the nM range.[19,20]

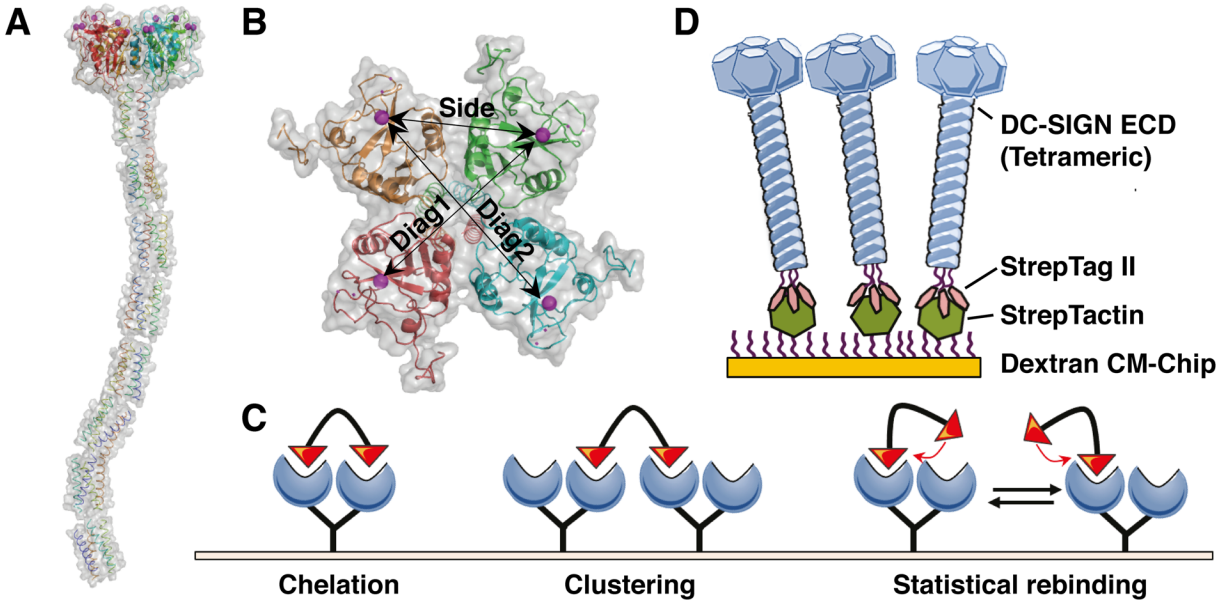

Figure 1. DC-SIGN extracellular domain as a tetrameric binding platform. A. Side view, combination of CRD structures and Neck model fitted into SAXS envelope of whole ECD.[9] B. Top view of tetrameric head. For clarity only the Ca^{2+} ions of the carbohydrate binding site are represented (magenta). The distance between 2 Ca^{2+} binding sites covers a length of ~39 Å between 2 adjacent sites (Side), ~51 Å and ~59 Å for 2 respective opposite sites (Diag1 and Diag2). C) Theoretical multivalent binding modes between a simplified bivalent ligand and a protein receptor with two binding sites (red triangle represents the "spearhead"): chelate effect (a), clustering effect (b), statistical rebinding (c)). D) The DC-SIGN oriented surface setup, via a *Strep*Tag/*Strep*Tactin coupling, for SPR measurements. It mimics the presentation and accessibility of binding sites on a cell surface and thus allows to observe the resultant of the different binding modes simultaneously.[20]

Multivalent effects can be of different types - statistical rebinding, clustering and chelation (Figure 1C). Over the past twenty years, researchers have shown an increased interest in synthesizing multivalent ligands,

especially for lectin binding,[21] which have often been built in a relatively unspecific fashion, privileging high-number valencies and relatively uncontrolled, flexible scaffolds. This type of design maximizes statistical rebinding effects and allows protein clustering in solution, while the occasional use of very large high-valency scaffolds[22,23] also capitalizes on the possibility of chelating simultaneously more than one CRD of the same (chelating) or different (clustering) lectin oligomer. However, the loss of flexibility upon binding generates unfavourable entropy.[24][25] An alternative strategy is thus to use smaller constructs of limited valency, which requires a careful design of the scaffold to meet the requirements for linker length and properties. It has been repeatedly shown that rigid linkers, unless exactly matched to the size of the receptor, are often too unforgiving of minor design inaccuracies and possibly not well-suited to the intrinsically flexible nature of proteins. Thus, an appropriate balance between rigidity and flexibility of the linker must be struck in order to maximize the possibility of binding events to occur productively and simultaneously in two or more protein binding sites, while minimizing the entropy costs. When this can occur, the level of avidity generated can yield several orders of magnitude as compared to that obtained by statistical rebinding effects only.[26]

We have previously shown this using a modular design that includes a linear rigid "rod-like" spacer of controllable length to connect two flexibles trivalent dendrons, each carrying 3 glycomimetic DC-SIGN ligands. The activity of the resulting constructs, as measured in DC-SIGN competition experiments and in a cellular model of DC-SIGN mediated HIV infection, was shown to depend on the length of the rod, the valency and the affinity of the monovalent ligand.[19,27] This study led to dendrimer **3.6** (Tab. 1, also called Polyman26), a nanomolar inhibitor of DC-SIGN mediated HIV transmission[19] which is internalized by dendritic cells and induce ß-chemokine and pro-inflammatory cytokine production.[11] More recently, Polyman26 also showed his capacity to inhibit, *in vitro* and in a cellular assay, the DC-SIGN-dependent trans-infection of the SARS-CoV-2 pseudo-virus as well as authentic SARS-CoV-2 virus.[7]

Here we collect interaction data obtained with several biophysical techniques for a series of rod-based constructs, including appropriate controls, in order to establish a detailed structure-activity relationship analysis of multivalent effects. Due to the multivalency in both the DC-SIGN tetramer and the hexavalent rod-like dendrimers, unraveling the complex and dynamic interaction required the use of several complementary techniques, which notably include a Surface Plasmon Resonance (SPR) oriented-DC-SIGN ECD surface methodology (Figure 1D) that we have recently developed.[20] These experimental approaches have been used in combination with theoretical methods and molecular modeling. The latter allowed us to consider, in the avidity mechanism, the role of the CRDs flexibility within the DC-SIGN tetramer. This variability of inter-CRDs distances has never been addressed in multivalent interaction studies up to now[28]. Altogether, it allowed us to gain structural and thermodynamic insights into the generation of avidity in this system and to define a new strategy for future development of other virus attachment blockers towards other C-type lectin receptors.

Results and discussion.

The full set of ligands analyzed is collected in Table 1. They all carry the modified pseudo-dimannoside **1** as the active spearhead. Dendrimers **1.6, 2.6** and **3.6** are all hexavalent and differ by the length of the spacer, which goes from one to three aromatic units (as indicated by the first digit in their numbering). Compounds **3.1, 3.2**, and **3.6** share the extended (3 units) rigid core, predicted from static model fitted to SAXS envelope to span two neighboring binding sites (~39 Å) (Figure 1B)[9], and are mono-, di- or hexa-valent (as indicated by the second digit in their numbering). Compound **3.6** corresponds to the previously shown optimum[19] of both valency and central core length.

Table 1. Schematic representation of rigid rod-based dendrimers and the K_{Dapp} values obtained by SPR on a DC-SIGN ECD oriented surface. IC_{50} values obtained in SPR inhibition experiments (from ref[19]) are included for comparison. Valency-corrected enhancement factors[13] (β) as compared to the modified pseudo-dimannoside spearhead **1** are shown. R=$CH_2CH_2OCH_2CH_2OH$ and R_1=$CH_2CH_2N_3$

Compounds	Structure	*Symbol*	IC_{50}[a] (μM)	$K_{D\ app}$[b] (μM)	ß factor
1	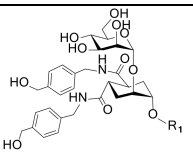		270	n.d.	-
3.1	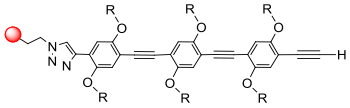		-	39.3 ± 3.9	-
3.2	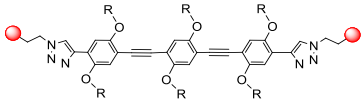		8	2.445 ± 0.25	8
3.2-long	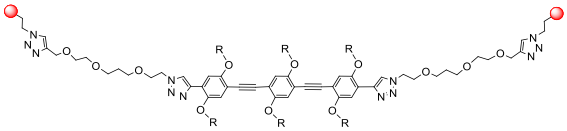		19	n.d.	
1.6	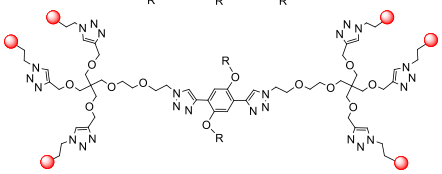		c	0.172 ± 0.028	38
2.6	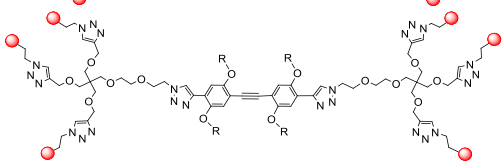		c	0.140 ± 0.008	47
3.6 Polyman 26	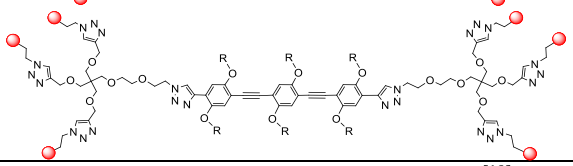		c	0.0115 ± 0.0023	570

a. From SPR inhibition study (competition experiment) (*ref* [19]) b. from SPR direct interaction measurement on a DC-SIGN ECD oriented surface (this work). c. IC50 values reported in ref[19] for these compounds was not significant (SPR competition experiment) because the lower limit of the test was reached.

Previously, these glycodendrimers were tested for their ability to inhibit binding of DC-SIGN ECD to immobilized BSA-Man or gp120 surfaces. However, we showed that in some cases, these SPR competition assay setting shows clear limitations as a tool for affinity determination,[20] due to the underestimation of surface-avidity phenomenon acting as a leading contributor of multivalent binding. In addition, in the case at hand, the lower limit of the inhibition assay sensitivity (affinity of the reporter interaction itself) was reached

for concentrations of the ligand in the low µM range. Thus, the system could be used to compare monovalent and divalent compounds (Table 1, compounds 1, 3.1, 3.2, 3.2-long and other in ref[19]), but failed to afford meaningful information for all the hexavalent presentations of **1**. In order to investigate the mechanism of these complex interactions, SPR analysis using DC-SIGN ECD-oriented surface corresponds to the most suitable approach. It mimics DC-SIGN presentation at the plasma membrane, with all CRDs accessible, but also the multivalent binding potential of the cell surface.[20] For the experiment, increasing concentrations of glycodendrimers were injected over the oriented surface. Sensorgrams are shown in Figure S1, $K_{D\ app}$ values are summarized in Table 1. Comparing the hexavalent series, reported in Figure 2A, the same range of affinity was observed between compounds **1.6** and **2.6**, with an apparent K_D ($K_{D\ app}$) of 0.17 and 0.14 µM respectively. On the contrary, an improvement by a factor of 10 was found for compound **3.6** with an affinity in the nM range ($K_{D\ app}$ = 11.5 nM), which compares well with the antiviral activity measured for this molecule in HIV and SARS-CoV-2 trans-infection assay.[7,19] This striking result confirms that the length of the rigid spacer is critical to improve binding affinity with DC-SIGN.

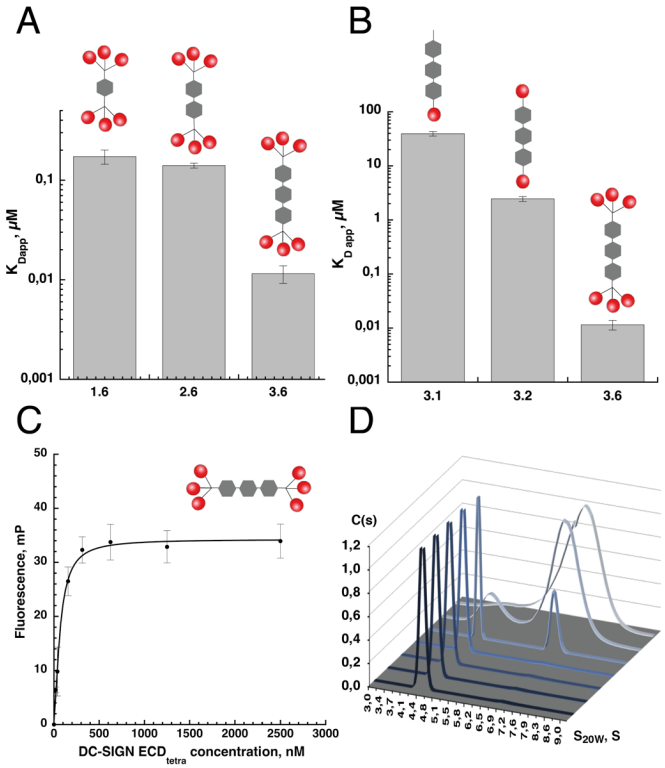

Figure 2: Binding properties of compound **3.6. A.** Comparison of K_{Dapp} values obtained by compounds titration over a DC-SIGN S-ECD surface. **B.** Comparison of K_{Dapp} values obtained by compounds titration over a DC-SIGN S-ECD surface. **C.** Direct binding assay using fluorescence polarization equilibrium measurements. Binding of compound **3.6** (400 nM) at increasing concentrations of DC-SIGN ECD tetramer (from 2.5 µM, serial dilution x2) are shown. **D.** Sedimentation velocity experiments of DC-SIGN tetramer alone (4 µM, black line) and with increasing compound **3.6** concentrations (0.005, 0.05, 0.5, 2, 4, 6 µM, from dark blue to light blue lines).

Figure 2B shows the role of valency for dendrimers sharing the same rod size. Remarkably, the K_D values of ligands **3.1** (39.3 ± 3.9 µM) , **3.2** (2.4 ± 0.25 µM) and **3.6** (11.5 ± 2.3 nM) show a regular increase of the affinity by one to two orders of magnitude as the valency increases from 1 to 2 to 6 for the same extended rigid core. There is a 6 fold factor between the IC_{50} and K_{Dapp} affinity measured for the spearhead **1** and for **3.1** (monovalent ligand conjugated to the extended rod). IC_{50} always underestimate affinity with respect to K_D,

suggesting that real affinity difference between **1** and **3.1** is probably lower than this factor 6, however it also suggests that the rod scaffold slightly contributes to the binding affinity. For this reason, compounds **3.1** will be used as monovalent ligand of reference to calculate the valency-corrected ß-factors. Indeed, a ß-factor of 8 is calculated for the divalent divalent ligand **3.2** (K_{Dapp}= 2.4 µM), suggesting that a chelation mechanism is now operative. The binding responses of **3.2** compared to its monovalent counterpart **3.1** (see Figure S1 and S2) highlight the multivalent binding properties of **3.2**. Figure S2 shows that while **3.1** display a hyperbolic 1:1 monovalent binding curve, **3.2** binding goes through a multivalent binding mode, chelation and/or clustering, in the µM range of concentration before it reaches a R_{max} half the value of the one of 3.1. The avidity is further boosted by increasing the ligand valency to six in **3.6** totaling to a valency-corrected ß-factor of 570 (Tab. 1). This occurs despite the entropy loss caused by the presence of an extended flexible linker in **3.6**, which we can estimate contributes by a negative factor of 2, as judged by comparison of the inhibition data for **3.2** and the **3.2-long** control obtained in ref[14] (see Table 2, entries 3 and 4). The affinity improvement from **3.2** to **3.6** (two orders of magnitude) reveals the positive effect of increasing the local concentration of ligand **1** at each extremity of the rigid spacer, probably due to statistical rebinding effects promoted locally at the level of each extremity (and the corresponding DC-SIGN binding sites). Thus, the cumulative effects of chelating/clustering and statistical rebinding modes are responsible for the high binding potency of **3.6**.

To further analyze the interaction mode of compound **3.6**, complementary biophysical solution-based approaches were used. Using the intrinsic fluorescence properties of the ROD spacer ($\lambda_{emission}$=430 nm/ $\lambda_{excitation}$=390 nm), a DC-SIGN ECD tetramer titration assay (Figure 2C), by fluorescence polarization (FP), confirms the nM range affinity (EC_{50}= 68 ± 8 nM). Interestingly, a plateau is reached for a **3.6**/DC-SIGN ECD stoichiometry around 1:1 (400 µM of both partner) suggesting an avidity mainly based on a chelation binding mode. A closer examination of the **3.6**/DC-SIGN tetramer binding process was performed by sedimentation velocity measurement at 4 µM of the DC-SIGN tetramer alone and with increasing concentrations of dendrimer (from 5 nM to 6 µM range) (Figure 2D). The present experiment revealed a first single species with an $S_{20,w}$= 4.7 S with a molar mass of 149 kDa. The peak is compatible with an elongated DC-SIGN tetramer. The same peak is observed for the DC-SIGN ECD solution alone and with concentrations of compound **3.6** going from 5 nM, to 500 nM. For higher concentrations (µM) of the compound, a second species appeared at an $S_{20,w}$= 7.3 S, corresponding to a dimer of DC-SIGN tetramers. The experiment shows that, as the ligand concentration reaches the µM range and approaches the protein concentration, clustering becomes a relevant binding mode, driven by the decrease of available DC-SIGN binding sites belonging to the same tetramer and suggesting an alternative mechanism of avidity generation in different concentration ranges of **3.6**.

Thermodynamic parameters of multivalent binding as measured by isothermal titration calorimetry (ITC) were analyzed for compounds **3.2** and **3.6**. The ITC binding analysis (Figure 3 and Table 2) is fully in agreement with the other biophysical techniques (see Table 2 for SPR and Figure 2C for FP of **3.6**) with K_D values equal to 58 ± 1 nM and 1.1± 0.2 µM for compounds **3.6** and **3.2** respectively. The enthalpy-driven association is significantly improved for compound **3.6** compared to **3.2** due to displaying of six copies of **1**,

rather than two, which drives the equilibrium toward the bound states. Increasing the local concentration close to the site is a major source of avidity generation. The ΔH difference is offset by a more unfavorable entropy for **3.6**, which can originate from the linker length and the loss of degrees of freedom of the construct extremities upon binding. Solvation may alos contribute, since the hydrophobic rod is shielded better from the solvent by the six units of ligand **1** in **3.6**[29] and thus it must pay a higher entropy penalty to attain the extended state necessary for multivalent binding. Combining the enthalpy and entropy effects, the ΔG for the hexavalent ligand improves by 10 kJ/mol. It is interesting to note that a stoichiometry of 1 for the complex with 3.6 is observed, supporting again the chelation mode. On the contrary, a stoichiometry n=1.5 is observed for **3.2**, with a K_{Dapp} in the µM range, which is compatible with a mixed chelation and clustering binding mode. Again, clustering is observed here in the µM range, as observed for **3.6** by analytical ultracentrifugation (Figure 2E), suggesting that this binding mode, at least in solution, appears at a specific relative ratio of concentration between DC-SIGN and the ligands.

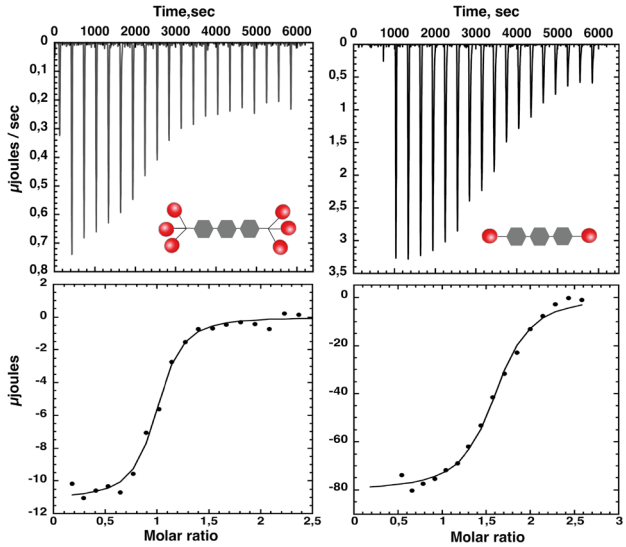

Figure 3: Thermodynamic parameters of multivalent binding as measured by isothermal titration calorimetry. Titration calorimetry of compound **3.6** (30 µM, left panel) and compound **3.2** (375 µM, right panel) in a cell containing DC-SIGN tetramer (respectively 30 µM and 48.75 µM).

Table 2: Thermodynamic data

Compounds	K_{Dapp}(nM)	ΔG, kJ/mol	ΔH, kJ/mol	TΔS, kJ/mol	n
3.2	1100 ± 200	-30.87	-85.27 ± 4.48	-54.4	1.56 ± 0.04
3.6	58 ± 1	-41.28	-146.98 ± 6.03	-105.7	0.96 ± 0.03

Thus, the data discussed so far support the view that both the length of the rod and the overall valency of the material have an influence on the affinity values. For a rod of optimal length, the affinity increases by one orders of magnitude when chelation becomes attainable (**3.1** vs **3.2**) and two orders of magnitude when statistical rebinding effects become operative in the context of chelation (**3.2** vs **3.6**). However, the affinity dependence on the rod size in the series **1.6, 2.6 3.6** and its brusque increase by 2 orders of magnitude when reaching **3.6** demand further explanation. Additionally, the sedimentation velocity experiments suggest that

protein clustering may become a significant binding mode in the appropriate relative concentration range of ligand and lectin.

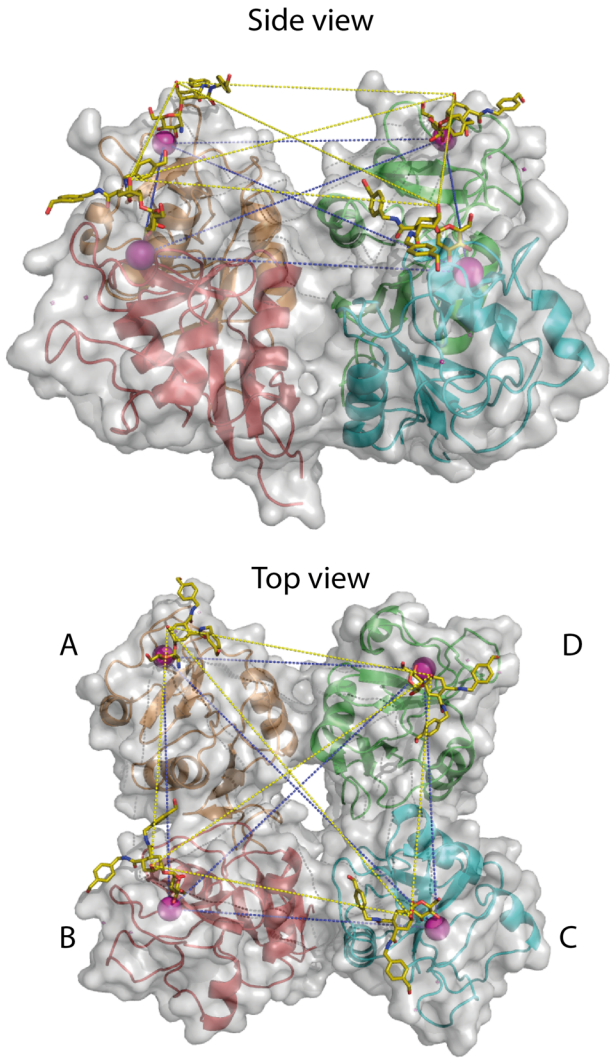

Figure 4. Distances between binding sites within tetrameric head of DC-SIGN. Tetrameric Model with compound **1** in each CRDs. This model derived from combination of SAXS envelope of DC-SIGN ECD[9], PDB: 6GHV[15] for glycomimetic/CRD complex and STD-NMR data for **1**[12]). Distances between $Ca^{2+}\cdots Ca^{2+}$ and OBG···OBG (OBG is the anomeric oxygen atom of 1) are represented by dark blue or yellow lines respectively. In the top view, CRDs are identified by letters from A to D (corresponding to orange, red, cyan and green cartoons respectively), allowing reference to the corresponding distances in Table 3 for this static model. For clarity, only the Ca^{2+} atoms of the carbohydrate binding sites are shown (magenta).

Table 3. The $Ca^{2+}\ldots Ca^{2+}$ and OBG···OBG distances measured in the model of the DC-SIGN tetramer/**1** complex (Å). OBG is the oxygen atom of **1** (EZ8 residue in compound 16 from [15]).

Distance (Å)	Ca-Ca (static)	OBG-OBG	diff	Ca-Ca (dynamic)
Side				
AB	40.3	36.7	3.6	46.9
AD	40.3	39.9	0.4	
BC	38.7	37.1	1.6	
CD	39.4	35.3	4.1	
Diag				
AC (Diag 2)	59.9	56.8	3.1	71.6
BD (Diag 1)	52.1	48.3	3.8	58.7

To gain structural insights into the possibilities of multivalent binding, we modeled the chelating binding modes attainable by compounds **1.6, 2.6** and **3.6** in the DC-SIGN tetramer. In the static model,[9] we distinguish three types of $Ca^{2+}\cdots Ca^{2+}$ distances in the DC-SIGN CRDs to be bridged by the compounds (Figure 1B; Table 3): a *Side* distance around 40 Å and two different diagonal distances *Diag1* (52 Å) and Diag2 (60 Å). From a practical point of view, the **1**: OBG···OBG distances, where OBG is the anomeric oxygen atom of **1** were used, to provide a comparison with the structure of the unbound ligand and an anchor point for a direct through-space linking. The OBG···OBG distances is at most 4.1 Å shorter than the respective $Ca^{2+}\cdots Ca^{2+}$ distances (Figure 4 and Table 3). Coupling this difference with the maximal OBG···OBG distances of **1.6, 2.6.** and **3.6** compounds obtained from their high-temperature dynamics in implicit solvent of 45.5, 52.0, and 58.6 Å, respectively, we arrive at the chelating potential (i.e. maximal $Ca^{2+}\cdots Ca^{2+}$ distance which can be bridged) of 49.6, 56.1 and 62.7 Å, respectively (Figure 5). This would mean that **1.6** would only be capable to bind in the *Side* mode, **2.6** would add *Diag1* and **3.6** could use all three binding modes (Figure 5 top; Figure 6).

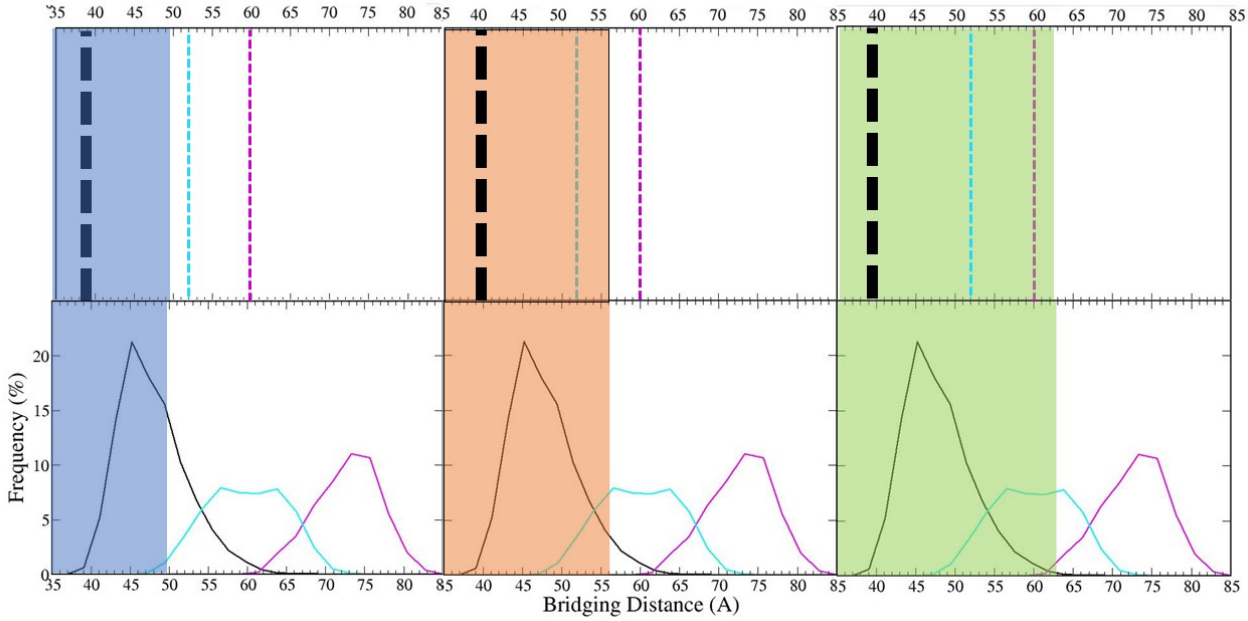

Figure 5. Bridging Ca…Ca distances in DC-SIGN tetramer. Static (dashed lines, top) and populations of dynamic (solid curves, bottom) distances are colored black for *Side* (left), cyan for *Diag 1* (middle) and magenta for *Diag2* (right). The chelating potential of **1.6, 2.6** and **3.6** compounds are shown as colored boxes (blue, orange and green, respectively).

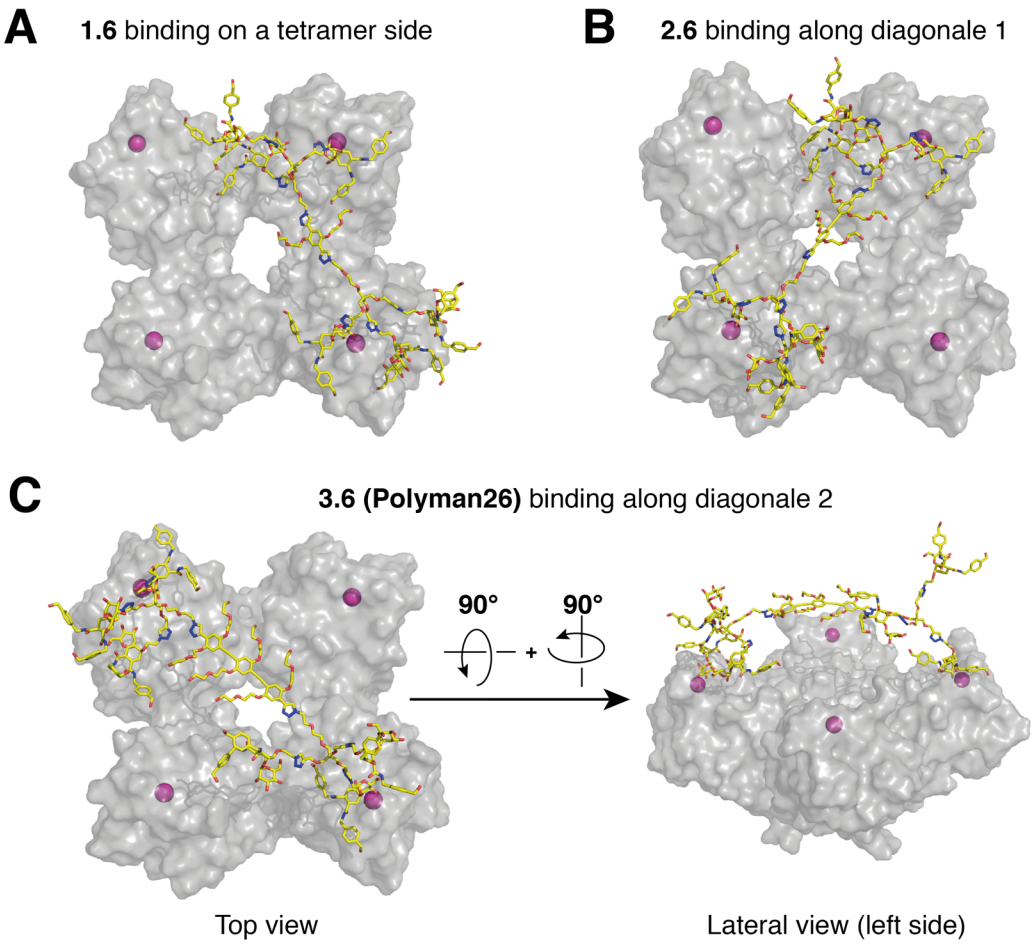

Figure 6. Computational models for a selection of chelation binding modes of rod-based dendrimers (in CPK colored sticks) on tetrameric DC-SIGN head. **A.** Chelation binding of **1.6** on the *Side,* **B.** Chelation binding of **2.6** along *Diag1,* **C.** Chelation binding of **3.6** (Polyman 26) along *Diag2.* Tetrameric head of DC-SIGN is represented in a surface mode and in the same orientation as in Figure 4. For clarity, only the Ca^{2+} atoms of the carbohydrate binding sites are represented (magenta).

A more realistic picture arises from a dynamic description of the DC-SIGN tetramer. Contrary to many other multivalent lectins, whose carbohydrate binding sites have a fixed geometry, relative movements of the four CRDs within the tetrameric DC-SIGN are possible and have been demonstrated previously[9,30]. They are enabled by the flexible link connecting the CRDs to the neck. It is thought that such flexibility is at the root of DC-SIGN capabilities to recognized and adapt to a wide repertoire of pathogens glycans whereas other lectin receptors, with fixed site spacing, recognize limited molecular patterns. Strikingly, this flexibility, and thus inter-CRDs distances variability, is rarely taken into consideration within the plethora of work aiming at designing multivalent ligand targeting DC-SIGN. In order here to evaluate its impacts in the avidity observed, the conformations attained during 2 µs of molecular dynamics simulation (MD) of the DC-SIGN tetramer/neck model are shown in Figure 7 (see also in Supplementary material Movie S1 and S2).

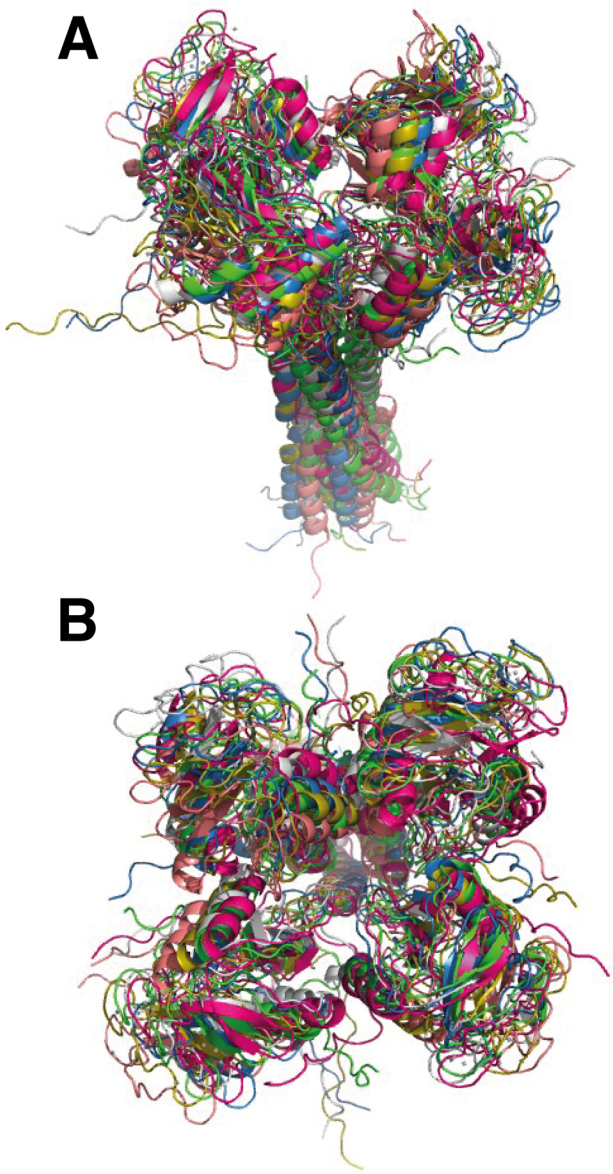

Figure 7. Snapshots from the 2µs MD of DC-SIGN tetramer A. Side view, B**.** top view. For better visualization of DC-SIGN dynamic, see movieS1 and S2.

The average CRD separations (measured as the $Ca^{2+\cdots}Ca^{2+}$ distances) from MD are by 7-12 Å larger than those in the average low-resolution SAXS model (Table 3). Considering less populated DC-SIGN tetramer conformations, the difference can increase up to 22-26 Å (Figure 5 bottom; solid curves). Thus, both **1.6** and **2.6** would capture a large portion of the *Side* binding modes (78 and 97 %, respectively) but only a small percentage of *Diag1* ones (1 and 19 %, respectively) and no *Diag2* ones. On the contrary, the longer **3.6** can capture not only all the *Side* binding modes but also 37 % of *Diag1* binding modes and it also starts to capture the shortest dynamic *Diag2* binding modes (Figure 5 and 6)).

While all data point toward a combination of statistical binding and chelation, improved by CRDs flexibility, as a source of the nM avidity range for the compound **3.6**, still, a protein clustering effect also remains a possibility. Such clustering mode have been observed here in the µM range of affinity, in AUC experiments, where DC-SIGN ECD is in solution. Such clustering can also occur on the surface of cell membranes, due to

the lateral mobility of the embedded tetramers and is used by glycosylated enveloped viruses whose particle size can bridge easily several receptors on the surface. It requires proximity and thus high-density of DC-SIGN receptor. The similar avidity values obtained comparing results in solution from FP and ITC on one side and direct interaction with oriented surfaces in SPR on the other side (where clustering mode could have been favored) argues here for a marginal effect of clustering in **3.6** avidity, at least in the conditions tested here. We have elaborated some theoretical thoughts regarding the potential clustering abilities of the various rod-based dendrimers toward hypothetically theoretical dense DC-SIGN-surfaces, which are shared within the supplementary material section. These considerations suggest that for these rod-dendrimers, which can span a distance far smaller than a virus particle, clustering events will not significantly account for the avidity properties towards lectins receptors in this context.

We note that the presented modeling of chelation has limitations due to the large size and flexibility of the DC-SIGN tetramer (such as insufficient sampling of mutual CRD arrangements in MD or static differences between $Ca^{2+}\cdots Ca^{2+}$ and OBG$\cdots$OBG distances). Nevertheless, the dynamical description in the chelation modes represents a significantly enhanced approach and offers qualitatively different views on the mutual spatial arrangements of the binding sites of multimeric DC-SIGN lectin and thus opens up new possibilities of explaining and exploring the avidity of multivalent ligands.

Conclusion

These studies have shown that rigid rod spacers of controllable length can be used to decipher multivalent binding modes responsible of avidity. Combining a range of techniques (partners in solution or immobilized) and molecular modelling, we highlighted the mechanisms behind the binding potency of **3.6,** a tight binder for DC-SIGN. The different features of rod dendrimers provide empirical insights to understand the correlation between each binding mode (chelating, rebinding and clustering effects) and the avidity production. In this specific case-study, the cumulative chelating and statistical rebinding modes make the huge difference for the compound **3.6** to become potent antagonist, as compared to other optimized multivalent glycoclusters targeting DC-SIGN tetramer. To achieve this goal, an extended rigid core was essential not only to cover part of the distance between adjacent site but also to favor sufficient extension of the structure in solution to potentiate binding. Finally, we showed that in the context of flexible carbohydrate recognition domain, the size of the ROD is also essential to increase the possibility of chelation binding and thus the net avidity.

Recently, we have shown that DC-SIGN and L-SIGN are attachment factors of SARS-CoV-2 virus and contribute to the infection[7] Many other studies have followed, confirming these observations and even suggesting that these lectins receptors could be primary receptors on their own and also contribute to immune dysregulation during SARS-CoV-2 infection.[31–34] In that context, we also demonstrated that Polyman26 (compound **3.6** in this work) could be used in cellular assay to inhibit DC-SIGN dependent trans-infection of SAR-CoV-2 virus[7].

The rigorous deciphering of the binding of **3.6** should help to improve the design of multivalent compounds and to predict the avidity generation of promising antagonists of DC-SIGN and, more broadly, of other

oligomeric receptors. In the context of the SARS-CoV-2 infection, L-SIGN could be a next target of interest since it is present at the surface of ACE2+ endothelial cell and is suggested to play a role as a co-receptor[31]. Next generation of improvement can be based on higher affinity monovalent ligands, higher valency but also scaffold geometry. We have already started to develop mimetic targeting L-SIGN and not only DC-SIGN[35]. However, aside to the ligand selectivity, the topological aspects underlined here are an important source of explanation for the avidity differences between multivalent ligands. Recent work, using glyconanoparticles as binding probes have shown drastic difference of multivalent binding mechanisms between the two closely related tetrameric DC-SIGN and L-SIGN. While DC-SIGN shows a propensity to chelation binding mode, L-SIGN appears to generate intercross-linking binding modes (equivalent of clustering but in solution) towards the glyconanoparticles[36]. Thus, despite a closely conserved sequence between the two tetrameric lectins (77%), major structural differences in the CRD head presentations are involved in multivalency. This is in line with previous structural work attempting to define respective organization of DC-SIGN and L-SIGN tetramers as a respectively "closing flower" or "open flower" models in which, the sugar binding sites are presented on top of the tetramer (DC-SIGN) or laterally (L-SIGN)[9,37]. Thus, targeting capacity towards L-SIGN may not only require new specific ligands but also an appropriate multivalent scaffold able to match to the specific topology of its CRDs. As for DC-SIGN, flexibility of CRDs within L-SIGN tetramers have been documented.[38] The strategy presented here to address the avidity towards DC-SIGN could be used to develop new virus-attachment blockers in the future for L-SIGN and others C-type lectins receptors of interest.

Acknowledgments:

This work used the platforms of the Grenoble Instruct-ERIC center (ISBG ; UAR 3518 CNRS-CEA-UGA-EMBL) within the Grenoble Partnership for Structural Biology (PSB), supported by FRISBI (ANR-10-INBS-0005-02) and GRAL, financed within the University Grenoble Alpes graduate school (Ecoles Universitaires de Recherche) CBH-EUR-GS (ANR-17-EURE-0003). M.L. has received funding for this project from the European Union's Horizon 2020 research and innovation programme under the Marie Sklodowska-Curie grant agreement No.795605, E.U. The work has been performed under the Project HPC-EUROPA3 (INFRAIA-2016-1-730897), E.U., with the support of the EC Research Innovation Action under the H2020 Programme; in particular, ML gratefully acknowledges the computer resources and technical support provided by EPCC at the University of Edinburgh, Scotland. M.L. was further supported by the project "Chemical Biology for Drugging Undruggable Targets" (ChemBioDrug CZ.02.1.01/0.0/0.0/16_019/0000729) from the European Regional Development Fund (OP RDE).

References

[1] T. B. Geijtenbeek, R. Torensma, S. J. van Vliet, G. C. van Duijnhoven, G. J. Adema, Y. van Kooyk, C. G. Figdor, *Cell* **2000**, *100*, 575–585.
[2] J. J. García-Vallejo, Y. van Kooyk, *Immunological Reviews* **2009**, *230*, 22–37.
[3] Y. van Kooyk, T. B. Geijtenbeek, *Nature reviews Immunology* **2003**, *3*, 697–709.
[4] N. Rahimi, *Biology* **2020**, *10*, 1.

[5] T. B. Geijtenbeek, D. S. Kwon, R. Torensma, S. J. van Vliet, G. C. van Duijnhoven, J. Middel, I. L. Cornelissen, H. S. Nottet, V. N. KewalRamani, D. R. Littman, C. G. Figdor, Y. van Kooyk, *Cell* **2000**, *100*, 587–597.
[6] C. P. Alvarez, F. Lasala, J. Carrillo, O. Muniz, A. L. Corbi, R. Delgado, *Journal of virology* **2002**, *76*, 6841–6844.
[7] M. Thépaut, J. Luczkowiak, C. Vivès, N. Labiod, I. Bally, F. Lasala, Y. Grimoire, D. Fenel, S. Sattin, N. Thielens, G. Schoehn, A. Bernardi, R. Delgado, F. Fieschi, *PLoS Pathog* **2021**, *17*, e1009576.
[8] H. Feinberg, D. A. Mitchell, K. Drickamer, W. I. Weis, *Science (New York, NY)* **2001**, *294*, 2163–2166.
[9] G. Tabarani, M. Thépaut, D. Stroebel, C. Ebel, C. Vivès, P. Vachette, D. Durand, F. Fieschi, *The Journal of biological chemistry* **2009**, *284*, 21229–21240.
[10] I. Sutkeviciute, M. Thépaut, S. Sattin, A. Berzi, J. McGeagh, S. Grudinin, J. Weiser, A. Le Roy, J. J. Reina, J. Rojo, M. Clerici, A. Bernardi, C. Ebel, F. Fieschi, *ACS chemical biology* **2014**, *9*, 1377–1385.
[11] B. Bertolotti, B. Oroszová, I. Sutkeviciute, L. Kniežo, F. Fieschi, K. Parkan, Z. Lovyová, M. Kašáková, J. Moravcová, *Carbohydrate research* **2016**, *435*, 7–18.
[12] N. Varga, I. Sutkeviciute, C. Guzzi, J. McGeagh, I. Petit-Haertlein, S. Gugliotta, J. Weiser, J. Angulo, F. Fieschi, A. Bernardi, *Chemistry (Weinheim an der Bergstrasse, Germany)* **2013**, *19*, 4786–4797.
[13] M. Andreini, D. Doknic, I. Sutkeviciute, J. J. Reina, J. Duan, E. Chabrol, M. Thépaut, E. Moroni, F. Doro, L. Belvisi, J. Weiser, J. Rojo, F. Fieschi, A. Bernardi, *Organic & biomolecular chemistry* **2011**, *9*, 5778–5786.
[14] V. Porkolab, E. Chabrol, N. Varga, S. Ordanini, I. Sutkevičiu Tė, M. Thépaut, M. J. García-Jiménez, E. Girard, P. M. Nieto, A. Bernardi, F. Fieschi, *ACS chemical biology* **2018**, *13*, 600–608.
[15] L. Medve, S. Achilli, J. Guzman-Caldentey, M. Thépaut, L. Senaldi, A. L. Roy, S. Sattin, C. Ebel, C. Vivès, S. Martin-Santamaria, A. Bernardi, F. Fieschi, *Chemistry – A European Journal* **2019**, DOI 10.1002/chem.201903391.
[16] J. Cramer, A. Lakkaichi, B. Aliu, R. P. Jakob, S. Klein, I. Cattaneo, X. Jiang, S. Rabbani, O. Schwardt, G. Zimmer, M. Ciancaglini, T. Abreu Mota, T. Maier, B. Ernst, *J. Am. Chem. Soc.* **2021**, jacs.1c06778.
[17] N. Varga, I. Sutkeviciute, R. Ribeiro-Viana, A. Berzi, R. Ramdasi, A. Daghetti, G. Vettoretti, A. Amara, M. Clerici, J. Rojo, F. Fieschi, A. Bernardi, *Biomaterials* **2014**, *35*, 4175–4184.
[18] M. Taouai, V. Porkolab, K. Chakroun, C. Chéneau, J. Luczkowiak, R. Abidi, D. Lesur, P. J. Cragg, F. Halary, R. Delgado, F. Fieschi, M. Benazza, *Bioconjugate chemistry* **2019**, *30*, 1114–1126.
[19] S. Ordanini, N. Varga, V. Porkolab, M. Thépaut, L. Belvisi, A. Bertaglia, A. Palmioli, A. Berzi, D. Trabattoni, M. Clerici, F. Fieschi, A. Bernardi, *Chemical communications (Cambridge, England)* **2015**, *51*, 3816–3819.
[20] V. Porkolab, C. Pifferi, I. Sutkeviciute, S. Ordanini, M. Taouai, M. Thépaut, C. Vivès, M. Benazza, A. Bernardi, O. Renaudet, F. Fieschi, *Org. Biomol. Chem.* **2020**, *18*, 4763–4772.
[21] A. Bernardi, J. Jiménez-Barbero, A. Casnati, C. De Castro, T. Darbre, F. Fieschi, J. Finne, H. Funken, K.-E. Jaeger, M. Lahmann, T. K. Lindhorst, M. Marradi, P. Messner, A. Molinaro, P. V. Murphy, C. Nativi, S. Oscarson, S. Penadés, F. Peri, R. J. Pieters, O. Renaudet, J.-L. Reymond, B. Richichi, J. Rojo, F. Sansone, C. Schäffer, W. B. Turnbull, T. Velasco-Torrijos, S. Vidal, S. Vincent, T. Wennekes, H. Zuilhof, A. Imberty, *Chemical Society Reviews* **2013**, *42*, 4709–4727.
[22] R. Ribeiro-Viana, M. Sánchez-Navarro, J. Luczkowiak, J. R. Koeppe, R. Delgado, J. Rojo, B. G. Davis, *Nature communications* **2012**, *3*, 1303.
[23] J. Ramos-Soriano, J. J. Reina, B. M. Illescas, N. de la Cruz, L. Rodríguez-Pérez, F. Lasala, J. Rojo, R. Delgado, N. Martín, *J. Am. Chem. Soc.* **2019**, jacs.9b08003.
[24] M. Mammen, S. K. Choi, G. M. Whitesides, *Angewandte Chemie \ldots* **1998**, *37*, 2754–2794.
[25] V. M. Krishnamurthy, V. Semetey, P. J. Bracher, N. Shen, G. M. Whitesides, *J. Am. Chem. Soc.* **2007**, *129*, 1312–1320.
[26] G. Bachem, E. Wamhoff, K. Silberreis, D. Kim, H. Baukmann, F. Fuchsberger, J. Dernedde, C. Rademacher, O. Seitz, *Angew. Chem. Int. Ed.* **2020**, *59*, 21016–21022.
[27] A. Berzi, S. Ordanini, B. Joosten, D. Trabattoni, A. Cambi, A. Bernardi, M. Clerici, *Scientific reports* **2016**, *6*, 35373.
[28] E. Zahorska, S. Kuhaudomlarp, S. Minervini, S. Yousaf, M. Lepsik, T. Kinsinger, A. K. H. Hirsch, A. Imberty, A. Titz, *Chem. Commun.* **2020**, *56*, 8822–8825.
[29] S. Ordanini, G. Zanchetta, V. Porkolab, C. Ebel, F. Fieschi, I. Guzzetti, D. Potenza, A. Palmioli, Č. Podlipnik, D. Meroni, A. Bernardi, *Macromolecular bioscience* **2016**, *16*, 896–905.

[30] S. Menon, K. Rosenberg, S. A. Graham, E. M. Ward, M. E. Taylor, K. Drickamer, D. E. Leckband, *PNAS* **2009**, *106*, 11524–11529.
[31] R. Amraei, W. Yin, M. A. Napoleon, E. L. Suder, J. Berrigan, Q. Zhao, J. Olejnik, K. B. Chandler, C. Xia, J. Feldman, B. M. Hauser, T. M. Caradonna, A. G. Schmidt, S. Gummuluru, E. Mühlberger, V. Chitalia, C. E. Costello, N. Rahimi, *ACS Cent. Sci.* **2021**, *7*, 1156–1165.
[32] Y. Kondo, J. L. Larabee, L. Gao, H. Shi, B. Shao, C. M. Hoover, J. M. McDaniel, Y.-C. Ho, R. Silasi-Mansat, S. A. Archer-Hartmann, P. Azadi, R. S. Srinivasan, A. R. Rezaie, A. Borczuk, J. C. Laurence, F. Lupu, J. Ahamed, R. P. McEver, J. F. Papin, Z. Yu, L. Xia, **n.d.**, 16.
[33] F. A. Lempp, L. Soriaga, M. Montiel-Ruiz, F. Benigni, J. Noack, Y.-J. Park, S. Bianchi, A. C. Walls, J. E. Bowen, J. Zhou, H. Kaiser, A. Joshi, M. Agostini, M. Meury, E. Dellota, S. Jaconi, E. Cameroni, J. Martinez-Picado, J. Vergara-Alert, N. Izquierdo-Useros, H. W. Virgin, A. Lanzavecchia, D. Veesler, L. Purcell, A. Telenti, D. Corti, *Nature* **2021**, DOI 10.1038/s41586-021-03925-1.
[34] Q. Lu, J. Liu, S. Zhao, M. F. Gomez Castro, M. Laurent-Rolle, J. Dong, X. Ran, P. Damani-Yokota, H. Tang, T. Karakousi, J. Son, M. E. Kaczmarek, Z. Zhang, S. T. Yeung, B. T. McCune, R. E. Chen, F. Tang, X. Ren, X. Chen, J. C. C. Hsu, M. Teplova, B. Huang, H. Deng, Z. Long, T. Mudianto, S. Jin, P. Lin, J. Du, R. Zang, T. T. Su, A. Herrera, M. Zhou, R. Yan, J. Cui, J. Zhu, Q. Zhou, T. Wang, J. Ma, S. B. Koralov, Z. Zhang, I. Aifantis, L. N. Segal, M. S. Diamond, K. M. Khanna, K. A. Stapleford, P. Cresswell, Y. Liu, S. Ding, Q. Xie, J. Wang, *Immunity* **2021**, S1074761321002120.
[35] S. Pollastri, C. Delaunay, M. Thépaut, F. Fieschi, A. Bernardi, *Chemical communications (Cambridge, England)* **2022**, In press.
[36] D. Budhadev, E. Poole, I. Nehlmeier, Y. Liu, J. Hooper, E. Kalverda, U. S. Akshath, N. Hondow, W. B. Turnbull, S. Pöhlmann, Y. Guo, D. Zhou, *J. Am. Chem. Soc.* **2020**, *142*, 18022–18034.
[37] H. Feinberg, C. K. W. Tso, M. E. Taylor, K. Drickamer, W. I. Weis, *Journal of molecular biology* **2009**, *394*, 613–620.
[38] D. E. Leckband, S. Menon, K. Rosenberg, S. A. Graham, M. E. Taylor, K. Drickamer, *Biochemistry* **2011**, *50*, 6125–6132.